Materials Science and Engineering A 528 (2011) 7589–7595

Contents lists available at ScienceDirect

Materials Science and Engineering A

journal homepage: www.elsevier.com/locate/msea

# Effect of oxide particles on the stabilization and final microstructure in aluminium

Andrea Bachmaier*, Reinhard Pippan

*Erich Schmid Institute of Materials Science – Austrian Academy of Sciences, Jahnstr. 12, A-8700 Leoben, Austria*

ARTICLE INFO

*Article history:*
Received 4 February 2011
Received in revised form 24 May 2011
Accepted 23 June 2011
Available online 29 June 2011

*Keywords:*
High pressure torsion
Aluminium
Alumina particles

ABSTRACT

Bulk aluminium samples containing alumina particles have been produced by different severe plastic deformation methods. Aluminium foils with different initial foil thicknesses were cold rolled to different amounts of strain and aluminium powders were consolidated and deformed by high pressure torsion (HPT). During processing, alumina particles from the foil or particle surface are easily incorporated and dispersed in the bulk material. The influence of these alumina particles on the developing microstructures and the mechanical properties has been studied.



## 1. Introduction

The mechanical and physical properties of materials are defined by structural features. A significant role plays the grain size of a material as the strength of a material increases with decreasing grain size which led to an increasing interest in producing materials with extremely small grain sizes [1]. Synthesis techniques are divided into "top-down" and "bottom-up" techniques as severe plastic deformation for the former one and such as inert gas condensation, electrodeposition, and ball milling with subsequent consolidation for the latter. Advantages of the top-down processes are that materials with theoretical density can be prepared, larger quantities of a material can be produced and contamination during the processing can be avoided.

Severe plastic deformation techniques include methods like equal channel angular pressing, HPT, multi-axial forging, constrained groove pressing and accumulative roll-bonding [1]. It has been shown that ultrafine grained and sometimes nanocrystalline materials can be obtained by severe plastic deformation of different metals and alloys, whereas the focus was mainly on the processing, microstructure and mechanical properties at equivalent strains of 1–10 [2–4]. At higher strains, a so called steady state is reached and no further refinement of the microstructure is possible [5]. The dominant process limiting the grain refinement is the occurrence of grain boundary migration during severe plastic deformation [5–8]. Therefore, all mechanisms reducing the mobility of grain boundaries are efficient to further decrease the grain size. This was shown for example in [6], where nanocrystalline nickel stabilized with homogeneously distributed nanometer-sized oxide particles was produced by HPT.

In a recent published study, the role of oxide particles on the development of deformation structures in pure aluminium containing a fine dispersion of oxides and of aluminium foil processed by rolling were investigated [9,10]. Consistently with our results for nickel, it was found that a finer scaled microstructure developed if the material contained oxides. The question arises how long these oxide particles are able to act as a barrier for grain boundary migration during processing. The present paper is devoted to this subject. Aluminium powders containing two different amounts of oxide particles are HPT deformed and the developing microstructure is compared to HPT deformed bulk aluminium. To prove the insignificance of the way how the strain is applied, layers of aluminium foil with different initial foil thicknesses were cold rolled to different amounts of strain and the role of the oxides on hindering grain boundary motion is studied. Furthermore, the thermal stability of the HPT deformed aluminium powder samples is investigated.

## 2. Experimental

In this study, aluminium of different initial conditions (powder, foil and bulk material) was processed by different severe plastic deformation methods.

Two different aluminium powders were used as starting material for HPT consolidation and subsequent deformation: aluminium powder (−325 mesh, 99.5% purity) was obtained from AlfaAesar®. The as-received aluminium powder has a mean particle size of

* Corresponding author. Tel.: +43 3842 804 314; fax: +43 3842 804 116.
*E-mail addresses:* andrea.bachmaier@stud.unileoben.ac.at (A. Bachmaier), reinhard.pippan@oaew.ac.at (R. Pippan).

0921-5093/$ – see front matter © 2011 Elsevier B.V. All rights reserved.
doi:10.1016/j.msea.2011.06.071

90 μm as measured from a series of scanning electron microscopy (SEM) images. A second aluminium powder was obtained from eckagranules® which has a mean particle size of 1.3 μm. Both aluminium powders were directly precompacted in our HPT tool without any special powder treatment or handling before the compaction. The powders were compacted to small disks with a diameter of ~8 mm and a thickness t of ~0.8 mm with a pressure of ~0.5 GPa. Afterwards, the precompacted samples were HPT deformed at room temperature for 25 rotations applying 4 GPa pressure. The rotation speed was kept constant at 0.2 rpm for all deformed samples. Further details of the HPT facility itself and the HPT deformation process are given in [4,5].

From a bulk aluminium (99.99% purity) rod, samples with a diameter of 8 mm and a thickness of 0.8 mm were cut. HPT deformation was conducted at room temperature for 3 turns with a pressure of 2 GPa.

Commercially available aluminium foil coils with an initial individual foil thickness $t_i$ of ~10–11 μm resulting in ~1500 layers of aluminium foil in one single coil were deformed by rolling in a single standard cold rolling mill without lubrication. The coils were cold rolled in one single pass to 50% thickness reduction to achieve adequate bonding. The gap was adjusted prior to rolling to give the designated reduction in thickness. Further cold rolling in several passes resulted in final thickness reductions of 78%, 90%, and 99%.

Aluminium foil (99.0% purity) with an initial thickness $t_i$ of ~750 nm and a variation in thickness of ±30% was obtained from Advent Research Materials. Stacks of ~600 layers (dimension of the sheets ~2 cm × 2 cm) of this submicron foil were cold rolled to estimated 75% and 85% thickness reductions in one single pass. Stacks of ~220 layers (dimensions of the sheets ~2 cm × 2 cm) of this foil were cold rolled in one single pass to estimated 90% thickness reduction and in one additional pass to an even higher thickness reduction (~95%). All stacks of the submicron aluminium foil were additionally enclosed in 2–4 layers of aluminium foil with a thickness of 10–11 μm to increase the complete starting thickness of the stacks. Due to the variation in thickness of ±30% and the additional outer thicker aluminium foils, the effective applied true strain can only be estimated.

All deformed samples were examined by SEM in a SEM type LEO 1525. In the case of the HPT deformed aluminium samples, the disks were cut in the middle and the micrographs were taken at radii of approximately 3 mm on the shear plane of the sample. All micrographs of the cold rolled aluminium foils were taken on the normal direction (ND)–rolling direction (RD) planes. Additionally, rectangles (dimensions ~10 μm × 10 μm) were milled on the ND–RD planes of the aluminium foil samples with an initial thickness of 750 nm cold rolled to the two highest thickness reductions (~90 and 95%) using a Focused ion beam (FIB) workstation (LEO XB 1540) by the impact of $Ga^+$ ions. To keep the FIB damage small the sample was cut perpendicular to the RD direction. The microstructure on these rectangles was examined by SEM right after FIB milling.

Grain sizes were measured from the SEM micrographs. About six or more representative BSE micrographs were chosen for the different aluminium powder samples and the aluminium foil samples with an initial foil thickness of 11 μm for all rolling conditions. The grains in each of the micrographs were traced by hand and the equivalent circle diameter (ECD) was defined from each material and condition. In the case of the aluminium foil samples with an initial foil thickness of 750 nm, the boundary spacing of the foils after the different degrees of rolling except for the aluminium foil with the highest reduction in thickness (~95%) were measured with the line intersection method from representative SEM micrographs.

Vickers microhardness measurements along the radii on the shear plane of the HPT deformed aluminium samples were performed on a BUEHLER Mircomet 5100 using a load of 200 g. Vickers microhardness tests using the same load as for the HPT deformed aluminium samples were performed on the RD–ND planes for the cold rolled aluminium foil samples with an initial thickness of 11 μm. For the aluminium foil samples with an initial thickness of 750 nm, Vickers microhardness tests using the minimum load of 10 g were performed on the RD–ND planes to avoid delamination of the aluminium foils. The mean values of 50 separated Vickers hardness measurements across the RD–ND planes for all aluminium foil samples are reported. However, it was not possible to evaluate the microhardness of the aluminium foil with higher thickness reductions with the Vickers microhardness test due to delamination of the individual foils. Therefore, indentations on the aluminium foil with approximately 90% thickness reductions were performed with a Hysitron TriboScope fitted with a Berkovich Indenter. 50 indentations measurements across the RD–ND planes were produced with a load of 2500 μN. For the purpose of comparison, indentations with the same alignments as mentioned before were additionally performed on the HPT deformed aluminium powder samples. On the sample with the highest amount of thickness reduction (~95%), 19 indentations with a load of 2500 μN were performed on the previously FIB milled rectangles.

The HPT deformed aluminium powder samples were additionally annealed in air for 1 h at 115–470 °C to investigate the thermal stability of the deformed material.

## 3. Results

### 3.1. Microstructure and microhardness of HPT deformed aluminium

HPT deformation of bulk aluminium and the HPT consolidation and deformation of the aluminium powders with the different initial particle sizes were performed until the saturation region was reached, meaning that no further grain refinement takes place [5]. Representative microstructures of the HPT deformed bulk aluminium sample and the HPT deformed aluminium powder sample with an initial particle size of about 90 μm can be seen in Fig. 1. Comparing both saturation microstructures, a huge difference in the final grain size is revealed. The average grain size of the HPT deformed bulk aluminium sample is ~1 μm (Fig. 1a). Compared to the bulk aluminium sample, the saturation microstructure of the HPT deformed powder aluminium sample has a significantly smaller grain size (Fig. 1b). The grain sizes were evaluated using several BSE micrographs: the mean grain size (ECD) was determined to be 145 nm for the Aluminium powder with the initial particle size of ~90 μm and 104 nm for the Aluminium powder with the initial particle size of ~1.3 μm. This means, the final microstructure of the aluminium powder samples consists of grains only about one tenth of the size of the HPT deformed bulk aluminium sample.

The large difference in the final microstructure of the different HPT deformed samples is also clearly visible in the measured microhardness values: the HPT bulk aluminium sample shows a nearly constant hardness along the radius with an average hardness of ~0.25 GPa (see Fig. 2). In the case of the aluminium powder samples the hardness values along the radius are considerably higher. The aluminium powder sample with the initial coarser particle size (90 μm) shows an average hardness of ~0.88 GPa which is more than 3 times the hardness of the HPT aluminium bulk sample. An even higher hardness is reached in the sample consolidated from the powder with the finer initial particle size (1.3 μm). With an average value of ~1.30 GPa, the hardness is more than 5 times higher than that of the HPT bulk aluminium.

Microhardness was measured from the center to the edge of the different HPT-deformed samples which implies that the applied strain increases from the center to the edge of the sample. There-

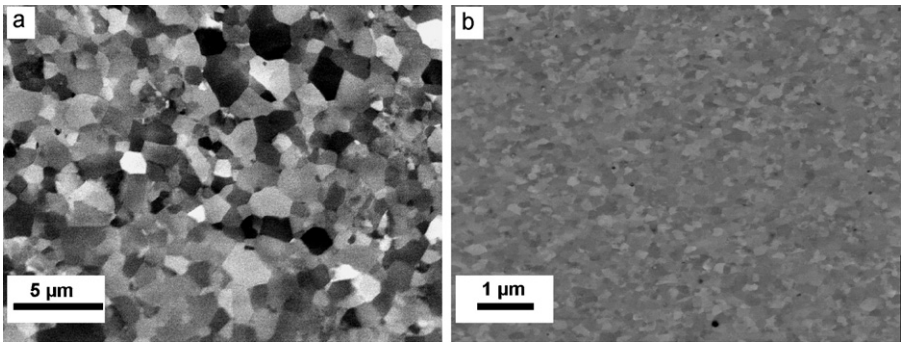


**Fig. 1.** (a) BSE micrograph of the saturation microstructure of a HPT bulk aluminium sample deformed at room temperature. (b) BSE micrograph of the saturation microstructure of a HPT consolidated and deformed aluminium powder sample with an initial aluminium particle size of about 90 μm.

fore, also the hardness should increase with increasing applied strain as well as the grain size constantly decreases. Nevertheless, there is a reasonable homogeneity in the hardness values across the center to the edge of the samples. If a high enough amount of strain is applied, a saturation region is reached where no further increase in hardness or decrease in grain size is observed. Due to the high amount of applied strain (25 revolutions), even at regions in approximate vicinity of the center this saturation region was easily reached.

### 3.2. Thermal stability of the HPT deformed samples

The HPT consolidated and deformed aluminium powder samples were additionally annealed for 1 h in air at temperatures up to about 0.8 $T_m$ ($T_m$ being the melting temperature) to evaluate the influence of subsequent annealing on the microhardness and microstructure. The annealing behaviour was investigated using microhardness testing after the annealing treatment. In Fig. 3, the measured microhardness as a function of the annealing temperature is plotted. For the HPT aluminium powder sample with the initial particle size of 90 μm, the hardness remains unchanged up to annealing temperatures of 0.60 $T_m$ (290 °C). At annealing temperatures of 0.77 $T_m$ (450 °C), a pronounced drop in the hardness is observable and a value of 0.73 GPa is measured. This drop in the hardness is connected to the beginning of grain growth which is confirmed by microstructural observations with the SEM. Until annealing temperatures of ~0.50 $T_m$ (200 °C), the hardness of the HPT aluminium sample with an initial particle size of 1.3 μm stays constant at a value of 1.3 GPa. At higher annealing temperatures the microhardness decreases constantly reaching values of 0.67 GPa at the highest annealing temperature of 0.8 $T_m$ (470 °C). In the beginning, the hardness decrease is due to recovery not affecting the grain size whereas at higher annealing temperatures grain growth occurs as well as approved by SEM.

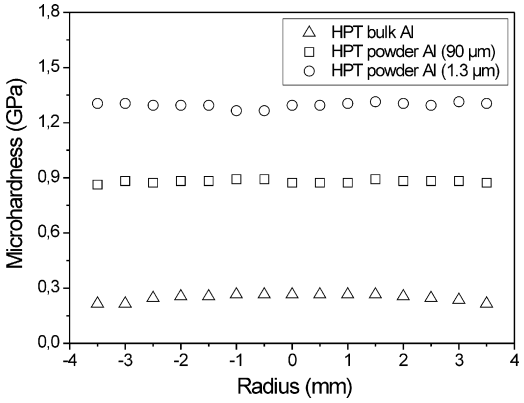


**Fig. 2.** Microhardness of HPT consolidated samples of aluminium powder with an initial particle size of about 1.3 μm and 90 μm and HPT bulk aluminium sample deformed at room temperature.

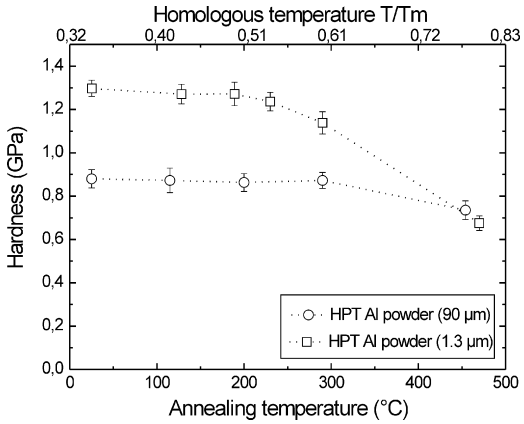


**Fig. 3.** Microhardness as a function of the annealing temperature for the HPT consolidated samples of aluminium powder with an initial particle size of 1.3 μm and 90 μm.

### 3.3. Microstructure and microhardness of the cold rolled aluminium foils

Stacks of aluminium foil with an initial foil thickness of ~11 μm were cold rolled in one single pass to 50% thickness reduction. This high amount of thickness reduction in the beginning was necessary to achieve sufficient bonding between the individual layers of the aluminium foil to enable further rolling. Several further passes resulted in overall thickness reductions of 78%, 90% and 99%. The data in Table 1 summarizes the ECD values, the original foil boundary spacing and microhardness values measured for the aluminium foils with the different thickness reductions. With increasing amount of strain, the distance between the original boundaries is reduced. As well as the thickness of the foils is decreasing, the grain size is reduced from 1.08 μm at 50% thickness reduction to 0.47 μm at 99% thickness reduction. The distance between the

**Table 1**
Applied thickness reduction, equivalent circle diameter (ECD), boundary spacing and microhardness for the aluminium foil with an initial thickness of 11 μm.

| Thickness reduction (%) | ECD (μm) | Boundary spacing (μm) | Microhardness (GPa) |
|---|---|---|---|
| 50 | 1.08 | ~5.1 | 0.35 |
| 78 | 0.75 | ~2.4 | 0.41 |
| 90 | 0.65 | ~1.1 | 0.43 |
| 99 | 0.47 | – | 0.47 |

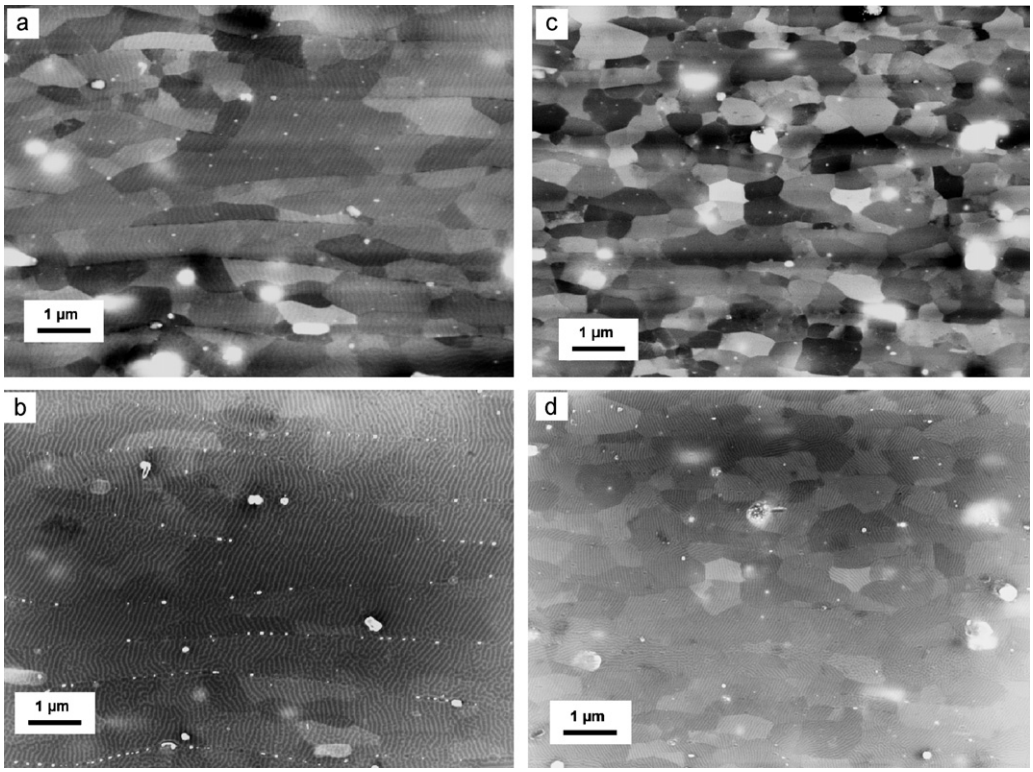


**Fig. 4.** BSE micrographs of the final microstructure of the cold rolled aluminium foils with an initial thickness of about 11 μm: (a) aluminium foil cold rolled to 90% thickness reduction and (c) aluminium foil cold rolled to 99% thickness reduction. SEM micrographs recorded with the inlens detector, (b) aluminium foil rolled to 90% thickness reduction and (d) aluminium foil cold rolled to 99% thickness reduction.

original boundaries decreases from about 5.1 μm at 50% thickness reduction to about 1.1 μm at 90% thickness reduction. At thickness reductions of 99%, the original foil boundaries are no longer visible. Microhardness increased from 0.35 GPa for the sample cold rolled to 50% thickness reduction to 0.47 GPa for the sample cold rolled to 99% thickness reduction. In Fig. 4, the resulting microstructures of the aluminium foil cold rolled to 90% and 99% thickness reduction can be seen. The wavy structures sometimes visible in Fig. 4 are artefacts from the electro-polishing treatment. Fig. 4a shows a BSE micrograph of the aluminium foil with 90% thickness reduction. The original boundaries between the individual aluminium foils are still visible and most of the grains are located between these boundaries. The grains seem to be a bit aligned in rolling direction. Due to the natural alumina layer which forms on the surface of the individual aluminium foils, alumina particles are incorporated in the aluminium matrix. The position of the original foil boundaries and the alumina particles can be more clearly seen in Fig. 4b, which shows a micrograph taken with the Inlens detector from almost the same area as in Fig. 4a. The alumina particles are aligned in the rolling direction emphasizing the original positions of the foil boundaries. The alumina particles influence the position of the boundaries. It seems that nearly no alumina particles are located between the original foil boundaries. The boundary spacing is also somewhat variable as the original foils are not perfectly straightened.

In Fig. 4c and d, BSE and In-lens micrographs of the aluminium foil cold rolled to 99% thickness reduction recorded at the same area can be seen. In contrast to the former microstructure, the original foil boundaries are no longer visible. Besides, the grains seem to be more equiaxed and hardly any alumina particles can be seen compared to the microstructure in Fig. 4a and b. Furthermore, the few still visible alumina particles seem to be located more inside the grains than on the grain boundary. One possible reason for the diminished number of visible alumina particles might be due to different etching times during sample preparation in the case of the aluminium foil samples cold rolled to 90 and 99% thickness reduction. Depending on the etching time and location of the alumina particles, there are apparently more or less alumina particles visible.

**Table 2**
Measured foil spacing and microhardness for the aluminium foil with an initial foil thickness of 750 nm.

| Thickness reduction (%) | Foil spacing (μm) | Microhardness (GPa) |
|---|---|---|
| ~75 | 0.174 | 0.62 |
| ~85 | 0.130 | 0.71 |
| ~90 | 0.107 | 1.44[a] |
| ~95 | <0.1, ~0.05 | 3.57[a] |

[a] Measured with nanoindentation.

Stacks of aluminium foil with an initial thickness of approximately 750 nm were cold rolled in one single pass to 4 different thickness reductions (approximately 75–95%). Table 2 summarizes the rolling conditions, resulting final foil spacing and microhardness of the cold rolled foils. Unfortunately it was not possible to prepare the samples metallographically adequate to record good SEM micrographs were the individual grains are visible. Nevertheless, it was possible to resolve the individual foils. The resulting foil spacing of each rolled condition was measured from several SEM micrographs using the line intersection method. The foil spacing decreases from 170 nm for the aluminium foil rolled to 75% thickness reduction to 107 nm in the case of the foil rolled to 90% thickness reduction. The SEM micrograph recorded at the previously FIB milled rectangle of the aluminium foil sample cold rolled to ~90% thickness reduction can be seen in Fig. 5a. Even though only the final thickness of the foils can be seen from the SEM micrographs, one can assume that the maximum possible grain size in the foils is limited by the foil thickness. Therefore, the maximum possible grain size in the foil with 90% thickness reduction is about 107 nm. In Fig. 5b, the microstructure of the aluminium foil sample

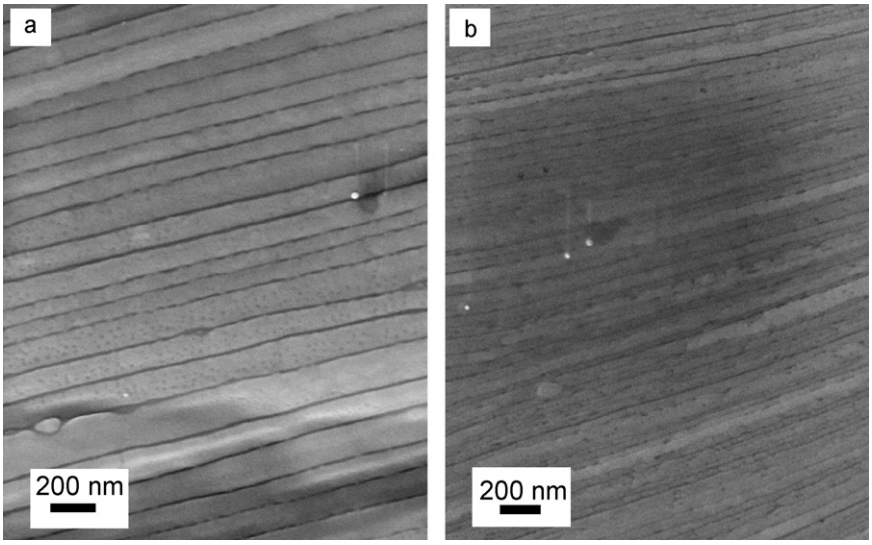


**Fig. 5.** (a) SEM micrographs of the final microstructure of the aluminium foil with an initial thickness of ~750 nm cold rolled to approximately 90% thickness reduction. (b) SEM micrograph of the final microstructure of the aluminium foil with an initial thickness of ~750 nm cold rolled to approximately 95% thickness reduction.

cold rolled to the highest thickness reduction can be seen. From the micrograph, final foil thicknesses definitely below 100 nm can be observed and the mean foil spacing is estimated to be around 50 nm. It can be assumed that the maximum possible grain size in this foil is limited by the foil thickness as well.

The hardness of the aluminium foils with an initial thickness of 750 nm increased from 0.62 GPa for the aluminium foil with the smallest amount of thickness reduction to about 3.57 GPa for the aluminium foil with the highest amount of thickness reduction.

## 4. Discussion

### *4.1. Effect of alumina particles on microstructure and thermal stability*

On the surface of the aluminium powders, initially an amorphous oxide film is formed which has a thickness somewhat below 4 nm at room temperature without any oxidation treatment [11,12]. Since no additional heat treatment was performed on our aluminium powders, we assume that on the surface of the powders an amorphous alumina film with a thickness of about 4 nm is formed. Based on the fact of different amount of surface area for different initial particle sizes, the fraction of alumina is distinctly higher for the aluminium powder with the smaller initial particle size.

During HPT consolidation and deformation, the powder particles undergo severe plastic deformation, they become elongated and the alumina layer fractures into small particles. These particles are distributed through the aluminium matrix as simultaneously the grain size is refined. The alumina particles have an influence on the structural evolution and final attainable grain size of the aluminium samples. Whereas in the HPT deformed bulk aluminium sample a saturation grain size of ~1 μm is obtained, the saturation grain size in the HPT deformed aluminium powder samples is ~100 to 150 nm depending on the initial particle size. We assume that a process similar to dynamic recrystallization limits the refinement during SPD [5,7]. Due to the pinning effect of the alumina particles on grain boundaries, therefore deterring recovery and recrystallization during the deformation, a significantly finer microstructure is obtained compared to bulk HPT deformed aluminium.

The thermal stability of a material is of great importance. Both samples exhibit inherent grain size stability up to reasonably high temperatures for pure aluminium or even aluminium alloys [13]. The hardness of both materials is stable up to an annealing temperature of ~200 °C. Recrystallization or grain growth is delayed because the finely dispersed alumina particles pin grain boundaries. Therefore, the thermal stability of the material can be considerably enhanced by these particles.

On the surface of aluminium foils an amorphous alumina film forms immediately as well [14]. Taking stacks of aluminium foils and rolling these stacks to produce an aluminium bulk sample gives the possibility to examine the effects of the alumina particles on the latter bulk sample. During the rolling process, the brittle alumina film fractures and is fragmented, whereas the aluminium is able to deform plastically. Assuming that the alumina particles formed are distributed through the aluminium by this rolling process, their influence on the microstructure and mechanical properties are easily analysed. Taking aluminium foils with an initial foil thickness of approximately 10 μm, the original grains can not exceed a size of 10 μm. Rolling these foils to 90% thickness reduction should lead to foil thicknesses of approximately 1 μm with grains not exceeding 1 μm. Even smaller grain sizes should be possible, if the same foils are rolled to even higher thickness reductions.

The alumina particles were observed to be located on the original boundaries of the aluminium foils cold rolled to 50%, 78% and 90% thickness reduction. Only at the highest strain in this study (99% thickness reduction), nearly no aligned alumina particles can be seen any more. It seems that with increasing strain, the pinning effect of the alumina particles reaches saturation. With increasing strain, the length of boundaries in the material increases by elongation of the grains or by the formation of new boundaries. On the contrary, the number of the alumina particles remains constant. At a certain amount of strain, the number of alumina particles gets insufficient to pin the boundaries effectively and the boundaries are able to disassociate themselves from the alumina particles more effectively.

Compared to pure aluminium processed by accumulative roll bonding to similar strains equivalent microstructures could be reached in our cold rolled foils [15,16]. It is hardly surprising because the roll bonding process of the aluminium foils is similar to the accumulative roll bonding process.

The pinning and stabilization effect by the oxide particles at the grain boundary to the reduced foil thickness remains until a thickness reduction of ~90 to 95% for both aluminium foils independent from their initial foil thickness of 11 μm or 750 nm. The same effect is also observed for the HPT consolidated and deformed

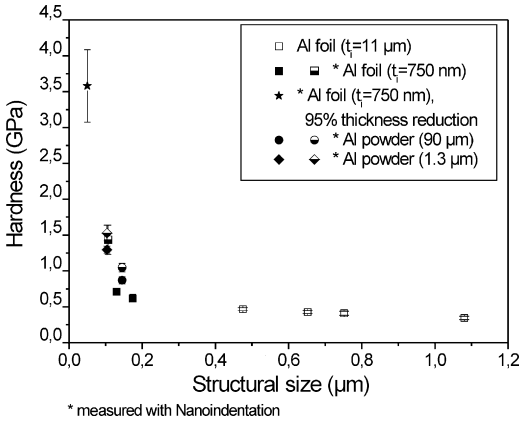


**Fig. 6.** Microhardness as a function of structural size plotted for the aluminium foils with an initial thickness $t_i$ of 11 μm cold rolled to 50%, 78%, 90% and 99% thickness reduction, the aluminium foil with an $t_i$ of 750 nm cold rolled to approximately 75%, 85%, 90% and 95% thickness reduction and for the HPT consolidated samples of aluminium powder with an initial particle size of 1.3 μm and 90 μm, respectively.

aluminium powder samples, where the grain size compared to HPT bulk deformed aluminium could be reduced and stabilized by a factor of ten.

### 4.2. Effect of alumina particles on strength

In Fig. 6, the hardness as a function of the structural size of the different aluminium samples is plotted. Structural size stands for the measured mean equivalent circle diameter in the case of the HPT deformed aluminium powder samples and the aluminium foil samples with an initial foil thickness of about 11 μm. For the aluminium foil samples with an initial foil thickness of 750 nm, structural size denotes the spacing between the individual foils measured with the line intersection method. In case of the aluminium foil sample with an initial foil thickness of 750 nm cold rolled to the highest thickness reduction (∼95%), the spacing between the individual foils could not be measured due to the small spacing distance and the mean foil thickness is estimated to be about 50 nm (compare SEM image of the microstructure in Fig. 5b).

In the beginning, the hardness of the samples continuously increases with decreasing structural size. As the structural size gets smaller, a deviation from the continuous hardness increase is observed and the hardness distinctly increases faster. Due to the fact that the hardness of the aluminium foil samples with an initial foil thickness of 750 nm cold rolled to ∼90% and 95% thickness reduction could only be evaluated with nanoindentation, the hardness of both HPT deformed aluminium powder samples were measured with the Vickers microhardness test as well as with nanoindentation for the purpose of comparison. The measured hardness values with the nanoindentation method are slightly higher for both HPT deformed aluminium powder samples compared to the values measured with the Vickers microhardness test (see Fig. 6). Although the hardness measured with nanoindentation cannot be absolutely compared with the Vickers microhardness test results, the general trend towards a deviation of the linear hardness increase with decreasing structural size is definitely determinable.

The well known Hall–Petch relationship:

$$\sigma_y = \sigma_0 + k_y d^{-1/2}, \tag{1}$$

where $\sigma_0$ and $k_y$ are material specific parameters, correlates the yield strength of a material with the size of the grains [17,18]. To estimate the fraction of strength enhancement due to grain size, the obtained data is analysed in terms of this relation. In Fig. 7a, the calculated yield stress $\sigma_y$ is plotted as a function of the inverse square root of the structural size and as a function of the inverse structural size of the different aluminium samples in Fig. 7b. The yield stress is calculated from the measured hardness values by the Tabor relation given in Eq. (2) [19]:

$$H_v = 3 \cdot \sigma_y. \tag{2}$$

For structural sizes above ∼150 nm, classical Hall–Petch behaviour is observed (Fig. 7a). Experimental values of 62 MPa and 0.06 for $\sigma_0$ and $k_y$ were found, respectively. Compared to data from literature for $\sigma_0$ and $k_y$, the determined values for the aluminium samples in this study are slightly higher [20]. The values from the literature were determined for coarse grained recrystallized aluminium. Therefore, increased $\sigma_0$ and $k_y$ values result from deformation induced structures. Not only the structural size contributes to the increased hardness but high dislocation densities and high internal stresses contribute to the hardness as well. A small contribution of oxide dispersion strengthening due the presence of alumina particles is also expected but the amount of $Al_2O_3$ is rather low [9,21–23]. A deviation from the classical Hall–Petch behaviour is observed for smaller structural sizes: at structural sizes below ∼150 nm, the Hall–Petch relationship breaks down. For these samples, calculated yield stress values are significantly higher than predicted by the Hall–Petch relation. The reason for the enhanced

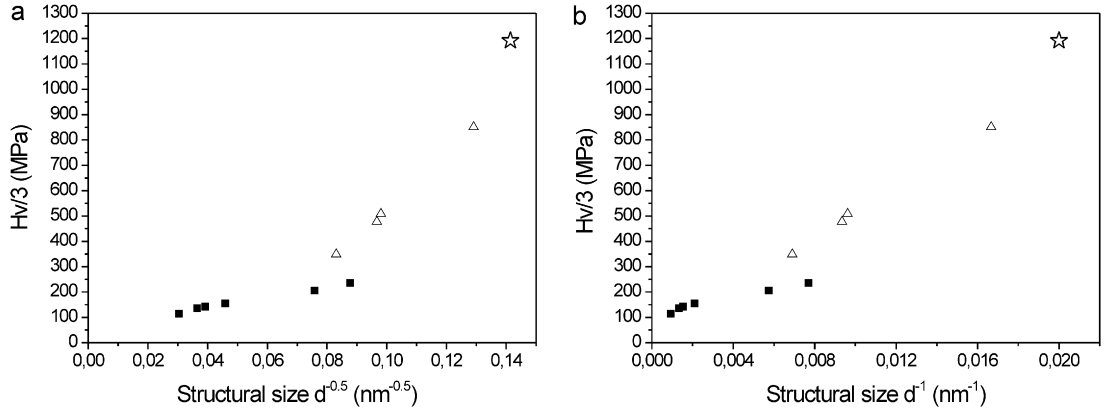


**Fig. 7.** (a) Yield stress plotted as a function of inverse square root of the structural size and (b) yield stress plotted as a function of the inverse structural size of all aluminium samples (filled symbols: aluminium foil samples with an initial thickness $t_i$ of 11 μm cold rolled to 50%, 78%, 90% and 99% thickness reduction and the aluminium foil with a $t_i$ of 750 nm cold rolled to approximately 75% and 85% thickness reduction; open symbols: HPY consolidated samples of aluminium powder with an particle size of 1.3 μm and 90 μm and the aluminium foil samples with an $t_i$ of 750 nm cold tolled to approximately 90% and 95% thickness reduction). The yield stress is calculated by the Tabor relation in both cases.

strength in this case cannot solely be attributed to the ultrafine structural size, the deformation induced structures and dispersion strengthening. The flow stress at large structural sizes is governed by dislocation motion. We assume that for small structural sizes, the activation or availability of dislocation sources is the determining factor controlling plasticity. Such a size controlled model is proposed to explain the enhanced yield stresses in thin films compared to their bulk counterparts as well [24,25]. This source controlled model predicts a yield stress that scales with the reciprocal of the film thickness. In our case the calculated yield stress should therefore scale with the inverse structural size at small sizes which matches with our aluminium sample results quite well as can be seen in Fig. 7b.

## 5. Conclusion

Aluminium samples containing dispersed alumina particles were prepared using two different SPD techniques. HPT consolidation and deformation of aluminium powders with two different amounts of alumina particles and cold rolling of layers of aluminium foil with different initial thicknesses were performed. Independent on the starting material and SPD technique, a significantly finer microstructure is obtained if the aluminium contains dispersed alumina particles. The fine grained microstructure is mainly induced by the pinning effect of the introduced alumina particles. Furthermore, it was found that independent of the initial grain size, which corresponds to the initial foil thickness or particle diameter, a reduction in size of the grains by a factor over ten can be achieved by the incorporation of the alumina particles. Accompanied with the reduction in the structural size, the hardness of the materials increased. The reported hardness data shows two different regions: (1) a region to a grain size of about 200 nm where classical Hall–Petch behaviour is found and (2) a region for grain sizes below 200 nm where the Hall–Petch relation roughly holds, but deviates from the classical −0.5 exponent. Furthermore, the HPT deformed aluminium samples exhibit reasonable grain size stability up to remarkable high temperatures for pure aluminium.

## Acknowledgments

The financial support by the Austrian Fonds zur Förderung der wissenschaftlichen Forschung (Project number: S10402-N16) is gratefully acknowledged. The author thanks Harald Lehofer for experimental assistance.

## References

[1] R.Z. Valiev, T.G. Langdon, Prog. Mater. Sci. 51 (2006) 881–981.
[2] R.Z. Valiev, R.K. Islamgaliev, I.V. Alexandrov, Prog. Mater. Sci. 45 (2000) 89–103.
[3] A.P. Zhilyaev, T.G. Langdon, Prog. Mater. Sci. 53 (2008) 893–979.
[4] R. Pippan, F. Wetscher, M. Hafok, A. Vorhauer, I. Sabirov, Adv. Eng. Mater. 8 (2006) 46–56.
[5] R. Pippan, S. Scheriau, A. Taylor, M. Hafok, A. Hohenwarter, A. Bachmaier, Annu. Rev. Mater. Res. 42 (2010) 319–344.
[6] A. Bachmaier, A. Hohenwarter, R. Pippan, Scr. Mater. 61 (2009) 1016–1019.
[7] A. Bachmaier, M. Hafok, R. Pippan, Mater. Trans. 51 (2010) 8–13.
[8] A. Bachmaier, R. Schuster, R. Pippan, Rev. Adv. Mater. Sci. 25 (2010) 1–8.
[9] C.Y. Barlow, P. Nielsen, N. Hansen, Acta Mater. 52 (2004) 3967–3972.
[10] C.Y. Barlow, N. Hansen, Y.L. Liu, Acta Mater. 50 (2002) 171–182.
[11] B. Rufino, F. Boulc'h, M.-V. Coulet, G. Lacroix, R. Denoyel, Acta Mater. 55 (2007) 2815–2827.
[12] M.A. Trunoc, M. Schoenitz, X. Zhu, E.L. Dreizin, Combust. Flame 140 (2005) 310–318.
[13] M. Lewandowska, K.J. Kurzydłowski, Mater. Charact. 55 (2005) 395–401.
[14] L.P.H. Jeurgens, W.G. Sloof, F.D. Tichelaar, E.J. Mittemeijer, Thin Solid Films 418 (2002) 89–101.
[15] C. Kwan, Z. Wangand, S.-B. Kang, Mater. Sci. Eng. A 480 (2008) 148–159.
[16] M. Eizadjou, H.D. Manesh, K. Janghorban, J. Alloys Compd. 474 (2009) 406–415.
[17] E.O. Hall, Proc. Phys. Soc. Lond. B 64 (1951) 747.
[18] N.J. Petch, J. Iron Steel Inst. 174 (1653) 25.
[19] G. Tabor, The Hardness of Metals, Clarendon Press, Oxford, 1951.
[20] N. Hansen, Acta Metall. 25 (1977) 863–869.
[21] N. Hansen, Scr. Mater. 51 (2004) 801–806.
[22] N.C. Kothari, J. Nucl. Mater. 41 (1971) 303–312.
[23] N. Hansen, Acta Metall. 52 (1970) 137.
[24] B. von Blanckenhagen, P. Gumbsch, E. Arzt, Philos. Mag. Lett. 83 (2003) 1–8.
[25] R. Venkatraman, J.C. Bravman, J. Mater. Res. 7 (1992) 2040–2048.